Title: Cholecystokinin input from the anterior cingulate cortex to the lateral periaqueductal gray mediates nocebo pain behavior in mice

Authors: Sandra J. Poulson[1], Aleksandrina Skvortsova[2], Lisiê V. Paz[1], Wanning Cui[1], Antonietta Mandatori[1], Jacob Burek[1], Fatama T. Zahra[3], Anton Dinh[1], Damien C. Boorman[1], Lianfang Liang[2], Jeffrey S. Mogil[2*], Loren J. Martin[1,3*]

Affiliations:

[1]Department of Psychology, University of Toronto Mississauga; Mississauga, Ontario, L5L 1C6, Canada.

[2]Department of Psychology, Anesthesia, and Faculty of Dental Medicine, and Alan Edwards Centre for Research on Pain, McGill University; Montreal, Quebec, H3A 1B1, Canada.

[3]Department of Cell and Systems Biology, University of Toronto; Toronto, Ontario, M5S 3G5, Canada.

*Corresponding author. Email: lj.martin@utoronto.ca and jeffrey.mogil@mcgill.ca

Abstract: The nocebo effect, the evil twin of the better-known placebo effect in which anticipation of harm causes that harm, is increasingly thought to be responsible for poor clinical outcomes. In humans, nocebo hyperalgesia (i.e., increased sensitivity to pain) is blocked by proglumide, a cholecystokinin (CCK) receptor antagonist. Yet the neural circuitry underlying nocebo hyperalgesia remains unidentified, largely due to lack of appropriate animal models. Independently, our two laboratories developed unique animal models of CCK-dependent nocebo hyperalgesia in which expectation of pain resulted from environmental or social cues. We find that both nocebo paradigms share a neural circuit involving CCK release from neurons projecting from the anterior cingulate cortex to the lateral periaqueductal gray. This pathway, which had not been previously recognized, could represent a promising target for therapeutic interventions in pain-related disorders.

One-Sentence Summary: Pain expectations, whether environmentally conditioned or transmitted socially, share a neural circuit, with cholecystokinin (CCK) projections from the anterior cingulate cortex (ACC) to the lateral periaqueductal gray (PAG) playing a pivotal role.

Main Text: Environmental, including social, cues are pivotal in shaping our perceptions of and responses to pain, influencing both placebo and nocebo effects [1-3]. Placebo analgesia arises when the positive expectation of pain relief triggers authentic analgesic outcomes, even without active painkillers—a concept widely explored in human studies [4-6] and recently in animals [7]. In the nocebo effect as it relates to pain, negative expectancies—created either by verbal suggestion, prior experience, or other contextual factors—lead to pain hypersensitivity or hyperalgesia [8]. Seminal work on nocebo hyperalgesia in humans by Benedetti and colleagues suggested that it was mediated by the peptide neurotransmitter cholecystokinin (CCK), as the CCK antagonist proglumide was able to abolish the effect (and potentiate placebo analgesia) in hidden injection experiments [9,10]. Very little is known about the biology of the nocebo effect beyond this due to the lack of appropriate animal models. However, mice can learn to have negative expectations through direct conditioning or via social learning from others. Both types of learning have been shown to produce nocebo hyperalgesia in humans [2,11].

We describe here experiments undertaken independently by two different laboratories, investigating the neurochemistry underlying nocebo hyperalgesia produced either by directly conditioning mice to a context where they previously received tonic pain [11,12] or by exposing mice socially to conspecifics who were actively in pain [13]. Thus, we hypothesized that environmentally conditioned or socially enhanced pain expectations rely on similar neural mechanisms that use cholecystokinin as a neurotransmitter. Using a combination of pharmacological, immunohistochemical, viral tracing, and optogenetic approaches, we show that both phenomena depend on the activation of CCK receptors. Furthermore, we define a neural circuit involving CCKergic neurons projecting from the anterior cingulate cortex (ACC) to the lateral periaqueductal gray (lPAG) that is crucial for nocebo hyperalgesia regardless of the paradigm producing it.

Inhibition of CCK receptors blocks nocebo pain hypersensitivity in mice

In humans, conditioning-based expectations have been demonstrated to induce nocebo hyperalgesia [14-16]. Thus, we posited that prior exposure to pain coupled with subsequent presentation of cues associated with that pain would generate a negative expectation, leading to heightened pain sensitivity in mice, a phenomenon dependent on the CCK system. To test this, we used a conditioned pain sensitivity protocol that consisted of a single pairing of an unconditioned (UCS; foot incision, **Fig. 1A** or surgical chronic constriction injury (CCI) of the sciatic nerve) and a conditioned stimulus (CS; environmental context). We tested whether unilateral hind paw incision and surgical chronic constriction injury (CCI) of the sciatic nerve could elicit conditioned pain sensitivity when returned to the same context 6 and 14 days later, respectively. When hind paw incision post-operative pain was used as the UCS (**Fig. 1A**), robust mechanical hypersensitivity averaged across hind paws was observed when mice were returned to the same (**Fig. 1B**), but not different context (**Fig. 1C**). There was no sex difference following hind paw incision (fig. S1, A – C) and CCI (fig. S1, D – F) conditioning. Despite the injuries being unilateral, mice exhibited increased bilateral nocebo hypersensitivity in response to hind paw incision (fig. S2) and CCI (fig. S3) conditioning. Conditioned pain sensitivity was blocked by systemic administration of proglumide when hind paw incision was used (**Fig. 1D**) and by LY225910 for both hind paw incision (**Fig. 1E**, fig S2) and CCI conditioning (fig. S3).

Since social cues, such as witnessing others in pain, also trigger nocebo hyperalgesia in humans [2,17] and facilitate pain in animals [13,18-21], we next sought to determine whether the CCK system also mediated the social enhancement of pain in mice. To address this, we adapted a one-in-pain social interaction assay where a naïve mouse (i.e., Pain Observer, PO) interacted with a cagemate displaying signs of visible pain from an intraplantar injection of formalin (i.e., Pain Demonstrator, PD). PO mice were then subsequently tested for pain responses (either chemical or

mechanical) in the absence of PD mice (**Fig. 1F**). After social interaction, PO mice exhibited increased hind paw licking in response to formalin injection compared to no pain observer (NPO) mice that interacted with a cagemate injected with saline (i.e., No Pain Demonstrator, NPD). Increased sensitivity in PO mice was blocked by systemic administration of proglumide (**Fig. 1G**).

Similarly, PO mice tested after interacting with a PD showed increased mechanical sensitivity (as measured on the electronic von Frey test) immediately after and 4 hours after but not 24 hours after the social interaction that was also blocked by systemic proglumide (**Fig. 1H**) and LY225910 (fig. S4). During the 30-min social interaction, PD mice displayed overt hind paw licking, while NPD mice displayed little to no hind paw licking (fig. S5A). During the social interaction, PO mice showed increased attending and propinquity (i.e., physical proximity) behavior toward PD mice compared to NPO mice (fig. S5, B and C) as well as anxiety-like behavior that was also blocked by pre-treatment with proglumide (fig. S5D). Metyrapone, a corticosterone synthesis blocker, did not block socially enhanced pain, suggesting that pain enhancement in this model is not dependent on stress (fig. S5E). Proglumide did not affect chemical (i.e., formalin) or mechanical sensitivity (fig. S5F) when mice were tested alone, indicating that proglumide alone does not affect baseline pain thresholds.

CCK receptors mediate nocebo hyperalgesia within the lateral periaqueductal gray

The PAG is active during a nocebo task in human participants, with increased activity observed in the lateral columns of the PAG more rostral than those areas showing placebo-responding activity [22]. For these next experiments, we aimed to demonstrate that activation patterns within the PAG were not specific to any model but indicative of the broader nocebo effect phenomenon. Thus, we used the conditioned pain (i.e., hind paw incision as the UCS) and social pain observation assays to characterize active (i.e., c-Fos^{+}) neurons within the PAG (**Fig. 2, A** and

B). A survey of the PAG across its rostrocaudal axis (**Fig. 2C**) revealed similar c-Fos$^+$ activation patterns for the contextual and the social nocebo assays. Specifically, the contextual and social nocebo assays showed no change in the precommisural nucleus (Prc), which is the most anterior portion of the PAG (aPAG, **Fig. 2D**). However, within the intermediate portion (imPAG; bregma -3.6 to -3.9 mm) of the nucleus, we observed increased c-Fos$^+$ neurons in the dorsomedial (dmPAG), dorsolateral (dlPAG) and lateral (lPAG) columns of mice returned to the same context (contextual nocebo) and in PO mice (social nocebo) (**Fig. 2E**), which was blocked by pre-treatment with proglumide in both paradigms. No apparent difference between the conditions for either assay was observed in the posterior PAG (pPAG; bregma -4.7 to -4.9 mm) in any of the columns (**Fig. 2F**). Representative images for c-Fos staining are shown for the imPAG for contextual and social nocebo in **Fig. 2, G** and **H**, respectively. Together, this indicates that the columns of the imPAG may be crucial for pain enhancement in contextual and social models of nocebo.

Next, we sought to determine whether CCK receptors in the intermediate dmPAG or lPAG were critical for nocebo pain behavior in mice. To do this, we cannulated mice in both regions and tested whether the application of proglumide interfered with contextual or social nocebo pain. We also infused CCK-8S into these regions to assess whether activation of CCK receptors was sufficient to evoke pain behavior. The intermediate dmPAG was selected due to its well-established role in sustained fear and anxiety states [23,24], while the lPAG was chosen for its involvement in social behavior [25] and pain processing [26]—both of which are highly relevant to nocebo pain behavior. Although we observed increased c-Fos$^+$ cells in the dlPAG of our nocebo groups, this region is predominantly associated with active defensive behaviors, such as escape, which are less relevant to nociceptive processing of social stimuli [27]. Mice infused with proglumide to the intermediate dmPAG continued to show enhanced pain behavior in the contextual and social nocebo models (**Fig. 3A – C**), while CCK-8S infusion in the intermediate dmPAG did not increase

sensitivity to mechanical stimulation (**Fig. 3D**) or responses on the hot-plate test (**Fig. 3E**). Conversely, proglumide infusion to the intermediate lPAG blocked pain hypersensitivity in both models (**Fig. 3F – H**). Application of proglumide to the intermediate lPAG did not affect the distance traveled or velocity in an open field test (fig. S6, A, and B), indicating a lack of motor effect that has been shown in other studies using systemically administered CCK antagonists [28]. Unlike the intermediate dmPAG, CCK-8S microinfusion into the intermediate lPAG increased mechanical sensitivity (**Fig. 3I**) and pain behavior on the hot plate test (**Fig. 3J**) and radiant heat paw-withdrawal test (fig S7, A and B).

Finally, we wanted to identify whether neurons in the PAG with increased c-Fos expression also expressed the CCK-2 receptor. The CCK-2 subtype of the CCK receptor is more abundant in the brain than the CCK-1 subtype [29] and is liberally present in the PAG [30]. Activation of CCK-2 receptors in the lateral column of the imPAG was confirmed using RNAscope, which revealed numerous neurons co-expressing *Fos* and *Cckbr* mRNA in both contextual (**Fig. 3, K and L**) and social (**Fig. 3, M and N**) nocebo.

Identification of long-range CCK projections that mediate nocebo behavior

To determine whether the source of CCK was projection neurons from another brain region, we infused a retrograde AAV specific for Cre that expressed mNeptune into the intermediate lPAG of CCK-IRES-Cre mice (**Fig. 4, A – C**). A small proportion of neurons expressing the retrograde tracer were found in some of the examined regions, including the insula, motor, retrosplenial, and parietal cortices (**Fig. 4, B and D**). However, we identified a unique set of CCK projection neurons with dense staining originating from the anterior cingulate cortex (ACC) (**Fig. 4, B and E**). These CCK^+ neurons, which project to the intermediate lPAG, appear to be confined to layer V of the ACC (**Fig. 4E**). Among the quantified regions, the ACC showed

a significantly higher expression of CCK^+ neurons compared to all other regions, as measured by the percentage of total NeuN staining in each region (**Fig. 4F**). Immunocytochemical visualization revealed that the retrogradely labeled CCK^+ neurons of the ACC are excitatory, as characterized by their co-expression of EMX1, a marker for excitatory neurons, and their pyramidal shape (fig. S8).

ACC → lPAG CCK projections are critical for nocebo pain behavior and pain sensitivity

Based on the microinfusion and viral tracing experiments, we hypothesized that CCK-expressing ACC neurons project to the lPAG to mediate nocebo pain behavior in mice. To test this, we injected an inhibitory opsin (eOPN3) into the right ACC, which expressed in terminal efferents in the intermediate lPAG, and implanted an optic cannula into the right lPAG (**Fig. 4G** and S9). After 3 weeks of expression, we tested whether optogenetically silencing CCK projections at the lPAG disrupted contextual or social nocebo responses (**Fig. 4, G-I**). Mice injected with the control virus showed enhanced sensitivity in the contextual (**Fig. 4H**) and social (**Fig. 4I**) nocebo pain models. However, mice injected with eOPN3 and stimulated with blue light no longer displayed enhanced sensitivity in either model (**Fig. 4, H and I**).

Because we showed that the CCKergic ACC→lPAG pathway is necessary for contextual and social nocebo, we further aimed to determine whether direct optogenetic activation of this pathway is sufficient to induce pain-like behaviors, specifically mechanical hypersensitivity. To target this pathway, we expressed channelrhodopsin-2 (ChR2) coupled to a mCherry tag in CCK neurons of the ACC using CCK-Cre mice and implanted an optical fiber above the lPAG (**Fig. 4J** and S10). Mice injected with AAVs containing only the mCherry tag served as controls. Optical stimulation of CCKergic ACC→lPAG neurons expressing ChR2-mCherry, but not those expressing mCherry, with blue laser light (470 nm, 20 Hz, 10 mW/mm^2) induced marked

mechanical hypersensitivity, as manifested by a drastic decrease in the threshold for the paw-withdrawal response induced by von Frey filaments (**Fig. 4K**). Robust CCKergic terminal expression was observed in the intermediate lPAG following viral infusion in the ACC (**Fig. S10**).

Discussion

Here, we demonstrate that a neural circuit releasing CCK from the anterior cingulate cortex (ACC) onto CCK-2 receptors in the lateral portion of the intermediate PAG is necessary and sufficient to produce hypersensitivity to both mechanical and thermal pain following two different nocebo paradigms in which expectation of pain is created either by classical conditioning or social learning. The rigor of this conclusion is enhanced by the independent but converging early work by two different laboratories, unaware of each other's findings. Furthermore, the fact that an identical neural circuit can be shown to underlie two paradigms with very different features, subjects, and measures suggests that the neural circuit is truly mediating what those paradigms have in common: nocebo hyperalgesia.

Our findings align with earlier studies showing that proglumide reduces nocebo hyperalgesia in people [10,31]. Notably, the specific blockade of conditioned pain by CCK-2, but not CCK-1 antagonists, underscores the specific role of the CCK-2 receptor subtype in nocebo pain hypersensitivity – a role that has been suspected but never demonstrated in human nocebo hyperalgesia. Importantly, systemic administration of proglumide did not change mechanical or thermal pain sensitivity when mice were tested outside of the nocebo paradigms, suggesting that proglumide specifically disrupts nocebo-induced pain sensitivity without affecting general pain processing. Further, in the social nocebo paradigm, observers interacting with a pain demonstrator exhibited cautious, anti-exploratory behavior on the elevated plus maze similar to previous

findings [32], which was reversed by proglumide. While CCK has been shown to play a role in anxiety in rodents [33-35], and people, [see 36 for a review], our study is the first to demonstrate that anticipatory anxiety due to a social context relies on CCK signalling. Moreover, our findings demonstrate that nocebos from multiple contexts are inherently anxiogenic and cultivate negative expectations in rodents, a concept previously suggested in human models [10,31,37].

While proglumide's effects on human nocebo hyperalgesia were reported decades ago[31], little progress has been made over the last 30 years in regard to clinical trials of CCK antagonists for anticipatory anxiety or as an opioid adjunct[38]. While some studies have shown positive results, the effects of proglumide on enhancement of opioid analgesia also appear to be inconsistent [39,40]. This may be due to proglumide's complex pharmacokinetics —characterized by third-order kinetics after oral administration, a rapid initial metabolism, and a prolonged elimination phase — which make it challenging to maintain stable therapeutic levels [41]. The efficacy of proglumide follows a bell-shaped dose-response curve, creating a narrow therapeutic window that complicates dosing and potentially reduces reliability [42]. The limited body of clinical evidence supporting its use as an opioid adjunct, coupled with regulatory hurdles, has also hindered its integration into standard clinical practice [43]. Our findings highlight the need for the development of more selective and potent CCK-2 receptor antagonists that can achieve therapeutic efficacy at lower concentrations. These advancements could mitigate off-target effects, enhance receptor specificity, and improve clinical outcomes for patients experiencing nocebo-related pain hypersensitivity or anxiety disorders. Developing such targeted pharmacological tools will be critical to translating our preclinical findings into viable clinical therapies.

The intermediate lPAG emerged as a critical region for nocebo pain behavior in our study. Increased c-Fos activation in the intermediate lPAG during both contextual and social nocebo

conditions and its blockade by proglumide pinpoint this region as a crucial hub for CCK-mediated nocebo pain effects. Our unique dataset provides an analysis of the PAG across coronal planes and along the anterior-posterior axis, revealing distinct PAG columns activated by our nocebo paradigms, extending beyond the typically studied posterior PAG. This mirrors findings from human fMRI studies, where neural activation in nocebo responders is localized to the lateral columns of the PAG, more rostral than placebo responders [22]. Although evidence from animal models in support of the role of the PAG in nocebo hyperalgesia has been limited, our findings, coupled with recent studies of conditioned and socially enhanced nausea behaviors in rats [44], highlight the significance of the PAG and its interconnected regions, such as the ACC, in nocebo effects.

The importance of the ACC in pain modulation is well-documented, particularly its involvement in affective components of pain and its connections to various pain processing regions, including the PAG. While the cortex is abundant with CCK-expressing interneurons, few CCK-expressing neurons in the cortex have long-range projections, and notable exceptions exist in the prelimbic cortex, ACC [45], and somatosensory cortex [46]. Among these regions, the ACC stands out for its specific projections to brain regions involved in the descending pain network [47,48]. While it had been previously shown that the ACC sends CCK projections to the thalamus [49], our work is the first to show CCK efferents from the ACC project into specific columns of the PAG. The ACC is well-known to project to the dlPAG and lPAG [50,51], which are PAG columns known to play key roles in enhancing reflexive and active pain avoidance behaviors [52]. Our work demonstrates that the predominately excitatory CCKergic projections of the ACC into the lPAG are crucial for mediating contextual and social nocebo responses. Silencing these CCKergic ACC→lPAG projections abolished nocebo pain responses, whereas optogenetic activation

induced mechanical allodynia, demonstrating the necessity and sufficiency of this pathway for nocebo pain behavior. This finding integrates well with existing literature on the role of the ACC in pain and emotional regulation [53], highlighting its ability to enhance pain expectations triggered by environmental and social learning. Although we acknowledge that excitatory CCKergic ACC neurons co-release other neurotransmitters, such as glutamate, this does not undermine the central role of CCK signaling in our observations. In fact, our proglumide experiments – both systemic and cannulation – clearly indicate that the observed nocebo pain effects are dependent on CCK receptor activity. The specificity of CCK's contribution to pain enhancement within this circuit could be further clarified with conditional knockout experiments targeting CCK or pharmacological blockade of CCK signaling in the lPAG during selective activation of CCKergic ACC projections. Additionally, the heterogeneity of CCK-2 receptor-expressing neurons in the lPAG, which likely include both excitatory and inhibitory subtypes, remains an intriguing area for future investigation to dissect their distinct contributions. This finding aligns with the broader literature on the ACC's role in pain and emotional regulation, emphasizing its ability to amplify pain expectations driven by environmental and social learning.

Placebo and nocebo effects are often viewed as opposites because they engage different neural and biochemical pathways. Placebo analgesia, for instance, can be disrupted by the opioid receptor antagonist, naloxone, demonstrating the involvement of endogenous opioids [54]. Conversely, in human models of nocebo hyperalgesia, increased pain responses are not reversed by naloxone [31]. Interestingly, application of the CCK-2 receptor agonist, pentagastrin, disrupts placebo analgesia in humans [55], while proglumide enhances placebo responses [10]. Since PAG activity during nocebo responses in humans [22] is found more rostral in the lPAG compared to placebo responses, the cells in this medial region of the PAG that express CCK-2 receptors (i.e.,

the *CCKBR* gene) may not co-express opioid receptors, and that may be the reason why naloxone does not affect the nocebo response. With the development of novel, robust, and convergent animal models (like those described here) to study these phenomena, more of these differences between placebo analgesia and nocebo hyperalgesia will likely be revealed.

The human relevance of our findings is enhanced by the reverse translational approach used, building on human pharmacological data. Evidence of human pain as a learning phenomenon continues to build [56], as does evidence for the social modulation of pain [57]. The prognosis of pain patients is worsened by sometimes inadvertent nocebo suggestions by clinical providers [58], and substantial psychological risk factors such as anxiety, harm avoidance, and pain catastrophizing can be conceptualized as an auto-nocebo process [59]. However, nocebo effects are largely greater in female subjects [60], wherein we did not observe stark differences between male and female mice in our nocebo models. This discrepancy may reflect species differences in baseline anxiety levels, hormonal regulation, or variations in experimental paradigms. Addressing these factors through comparative studies involving additional species, and human-like conditioning protocols will help clarify the observed differences and strengthen the translational applicability of our findings. Nonetheless, our integrated models of nocebo hyperalgesia, mediated by CCK-2 receptors and the ACC→lPAG pathway, provide a novel framework for understanding the neural basis of nocebo effects.

Overall, our findings have broader implications for developing targeted interventions to manage pain exacerbated by negative expectations and social factors. A better understanding of the neurobiology underlying the nocebo effect might have substantial implications for treating pain. More generally, these simple mouse models of nocebo pain hypersensitivity may prove invaluable in revealing that biology.

References and Notes

1 Testa, M., Rossettini, G., Barbiani, D. & Miciak, M. in *Placebo Effects Through the Lens of Translational Research* (eds Luana Colloca *et al.*) 0 (Oxford University Press, 2023).

2 Vogtle, E., Barke, A. & Kroner-Herwig, B. Nocebo hyperalgesia induced by social observational learning. *Pain* **154**, 1427-1433 (2013).

3 Colloca, L. & Benedetti, F. Placebo analgesia induced by social observational learning. *Pain* **144**, 28-34 (2009). https://doi.org/10.1016/j.pain.2009.01.033

4 Tracey, I. Getting the pain you expect: mechanisms of placebo, nocebo and reappraisal effects in humans. *Nat Med* **16**, 1277-1283 (2010). https://doi.org/10.1038/nm.2229

5 Benedetti, F., Mayberg, H. S., Wager, T. D., Stohler, C. S. & Zubieta, J. K. Neurobiological mechanisms of the placebo effect. *J Neurosci* **25**, 10390-10402 (2005). https://doi.org/10.1523/jneurosci.3458-05.2005

6 Zunhammer, M., Spisak, T., Wager, T. D., Bingel, U. & Placebo Imaging, C. Meta-analysis of neural systems underlying placebo analgesia from individual participant fMRI data. *Nat Commun* **12**, 1391 (2021). https://doi.org/10.1038/s41467-021-21179-3

7 Chen, C. *et al.* Neural circuit basis of placebo pain relief. *Nature* **632**, 1092-1100 (2024). https://doi.org/10.1038/s41586-024-07816-z

8 Colloca, L. The Nocebo Effect. *Annual Review of Pharmacology and Toxicology* **64**, 171-190 (2024). https://doi.org/https://doi.org/10.1146/annurev-pharmtox-022723-112425

9 Benedetti, F., Amanzio, M., Casadio, C., Oliaro, A. & Maggi, G. Blockade of nocebo hyperalgesia by the cholecystokinin antagonist proglumide. *Pain* **71**, 135-140 (1997).

10 Benedetti, F., Amanzio, M. & Maggi, G. Potentiation of placebo analgesia by proglumide. *Lancet* **346**, 1231 (1995).

11 Martin, L. J. *et al.* Male-Specific Conditioned Pain Hypersensitivity in Mice and Humans. *Current biology : CB* **29**, 192-201 e194 (2019). https://doi.org/10.1016/j.cub.2018.11.030

12 Trask, S., Mogil, J. S., Helmstetter, F. J., Stucky, C. L. & Sadler, K. E. Contextual control of conditioned pain tolerance and endogenous analgesic systems: evidence for sex-based differences in endogenous opioid engagement. *eLife* **11**, e75283 (2022).

13 Smith, M. L., Asada, N. & Malenka, R. C. Anterior cingulate inputs to nucleus accumbens control the social transfer of pain and analgesia. *Science* **371**, 153-159 (2021).

14 Bräscher, A. K., Kleinböhl, D., Hölzl, R. & Becker, S. Differential Classical Conditioning of the Nocebo Effect: Increasing Heat-Pain Perception without Verbal Suggestions. *Front Psychol* **8**, 2163 (2017). https://doi.org/10.3389/fpsyg.2017.02163

15 Tu, Y. *et al.* A neural mechanism of direct and observational conditioning for placebo and nocebo responses. *NeuroImage* **184**, 954-963 (2019). https://doi.org/10.1016/j.neuroimage.2018.10.020

16 Colloca, L., Petrovic, P., Wager, T. D., Ingvar, M. & Benedetti, F. How the number of learning trials affects placebo and nocebo responses. *Pain* **151**, 430-439 (2010). https://doi.org/10.1016/j.pain.2010.08.007

17 Saunders, C., Colagiuri, B. & Barnes, K. Socially Acquired Nocebo Effects Generalize but Are Not Attenuated by Choice. *Ann Behav Med* **57**, 1069-1080 (2023). https://doi.org/10.1093/abm/kaad056

18 Martin, L. J. *et al.* Reducing social stress elicits emotional contagion of pain in mouse and human strangers. *Current biology : CB* **25**, 326-332 (2015). https://doi.org/10.1016/j.cub.2014.11.028

19 Langford, D. J. *et al.* Social modulation of pain as evidence for empathy in mice. *Science* **312**, 1967-1970 (2006). https://doi.org/312/5782/1967 [pii] 10.1126/science.1128322

20 Lidhar, N. K. *et al.* Prelimbic cortex glucocorticoid receptors regulate the stress-mediated inhibition of pain contagion in male mice. *Neuropsychopharmacology* **46**, 1183-1193 (2021). https://doi.org/10.1038/s41386-020-00912-4

21 Li, Z. *et al.* Social interaction with a cagemate in pain facilitates subsequent spinal nociception via activation of the medial prefrontal cortex in rats. *Pain* **155**, 1253-1261 (2014). https://doi.org/10.1016/j.pain.2014.03.019

22 Crawford, L. S. *et al.* Brainstem Mechanisms of Pain Modulation: A within-Subjects 7T fMRI Study of Placebo Analgesic and Nocebo Hyperalgesic Responses. *J Neurosci* **41**, 9794-9806 (2021). https://doi.org/10.1523/JNEUROSCI.0806-21.2021

23 Borelli, K. G. & Brandao, M. L. Effects of ovine CRF injections into the dorsomedial, dorsolateral and lateral columns of the periaqueductal gray: a functional role for the dorsomedial column. *Horm Behav* **53**, 40-50 (2008). https://doi.org/10.1016/j.yhbeh.2007.08.013

24 Bandler, R. & Depaulis, A. in *The Midbrain Periaqueductal Gray Matter: Functional, Anatomical, and Neurochemical Organization* (eds Antoine Depaulis & Richard Bandler) 175-198 (Springer US, 1991).

25 Liu, Y. *et al.* A circuit from dorsal hippocampal CA3 to parvafox nucleus mediates chronic social defeat stress-induced deficits in preference for social novelty. *Sci Adv* **8**, eabe8828 (2022). https://doi.org/10.1126/sciadv.abe8828

26 Kaneko, T. *et al.* Orexin neurons play contrasting roles in itch and pain neural processing via projecting to the periaqueductal gray. *Commun Biol* **7**, 290 (2024). https://doi.org/10.1038/s42003-024-05997-x

27 Johnson, S. B. *et al.* Activity in a prefrontal-periaqueductal gray circuit overcomes behavioral and endocrine features of the passive coping stress response. *Proc Natl Acad Sci U S A* **119**, e2210783119 (2022). https://doi.org/10.1073/pnas.2210783119

28 Vasar, E., Lang, A., Harro, J., Bourin, M. & Bradwejn, J. Evidence for potentiation by CCK antagonists of the effect of cholecystokinin octapeptide in the elevated plus-maze. *Neuropharmacology* **33**, 729-735 (1994). https://doi.org/10.1016/0028-3908(94)90112-0

29 Moran, T. H., Robinson, P. H., Goldrich, M. S. & McHugh, P. R. Two brain cholecystokinin receptors: implications for behavioral actions. *Brain research* **362**, 175-179 (1986). https://doi.org/10.1016/0006-8993(86)91413-7

30 Lein, E. S. *et al.* Genome-wide atlas of gene expression in the adult mouse brain. *Nature* **445**, 168-176 (2007). https://doi.org/10.1038/nature05453

31 Benedetti, F., Amanzio, M., Casadio, C., Oliaro, A. & Maggi, G. Blockade of nocebo hyperalgesia by the cholecystokinin antagonist proglumide. *Pain* **71**, 135-140 (1997). https://doi.org/10.1016/s0304-3959(97)03346-0

32 Benassi-Cezar, G., Carmona, I. M., Baptista-de-Souza, D., Nunes-de-Souza, R. L. & Canto-de-Souza, A. Differential modulation of the anterior cingulate and insular cortices on anxiogenic-like responses induced by empathy for pain. *Neuropharmacology* **192**, 108413 (2021). https://doi.org/10.1016/j.neuropharm.2020.108413

33 Vazquez-Leon, P., Campos-Rodriguez, C., Gonzalez-Pliego, C. & Miranda-Paez, A. Differential effects of cholecystokinin (CCK-8) microinjection into the ventrolateral and dorsolateral periaqueductal gray on anxiety models in Wistar rats. *Horm Behav* **106**, 105-111 (2018). https://doi.org/10.1016/j.yhbeh.2018.10.003

34 Wang, H., Wong, P. T., Spiess, J. & Zhu, Y. Z. Cholecystokinin-2 (CCK2) receptor-mediated anxiety-like behaviors in rats. *Neurosci Biobehav Rev* **29**, 1361-1373 (2005). https://doi.org/10.1016/j.neubiorev.2005.05.008

35 Horinouchi, Y. *et al.* Reduced anxious behavior in mice lacking the CCK2 receptor gene. *Eur Neuropsychopharmacol* **14**, 157-161 (2004). https://doi.org/10.1016/s0924-977x(03)00103-2

36 Colloca, L. & Benedetti, F. Nocebo hyperalgesia: how anxiety is turned into pain. *Curr Opin Anaesthesiol* **20**, 435-439 (2007). https://doi.org/10.1097/ACO.0b013e3282b972fb

37 Benedetti, F. & Amanzio, M. The neurobiology of placebo analgesia: from endogenous opioids to cholecystokinin. *Prog Neurobiol* **52**, 109-125 (1997). https://doi.org/10.1016/s0301-0082(97)00006-3

38 Bernstein, Z. P., Yucht, S., Battista, E., Lema, M. & Spaulding, M. B. Proglumide as a morphine adjunct in cancer pain management. *J Pain Symptom Manage* **15**, 314-320 (1998). https://doi.org/10.1016/s0885-3924(98)00003-7

39 McCleane, G. Cholecystokinin antagonists: can they augment opioid-derived analgesia? *J Opioid Manag* **1**, 273-279 (2005). https://doi.org/10.5055/jom.2005.0057

40 Oliveira, D., Fontenele, R., Weleff, J., Sofuoglu, M. & De Aquino, J. P. Developing non-opioid therapeutics to alleviate pain among persons with opioid use disorder: a review of the human evidence. *Int Rev Psychiatry* **35**, 377-396 (2023). https://doi.org/10.1080/09540261.2023.2229430

41 Bignamini, A. A., Casula, P. L. & Rovati, A. L. Pharmacokinetic approach to proglumide long-term activity. *Arzneimittelforschung* **29**, 639-642 (1979).

42 Gay, M. D. *et al.* Proglumide Reverses Nonalcoholic Steatohepatitis by Interaction with the Farnesoid X Receptor and Altering the Microbiome. *Int J Mol Sci* **23** (2022). https://doi.org/10.3390/ijms23031899

43 Rabiee, A. *et al.* Safety and Dosing Study of a Cholecystokinin Receptor Antagonist in Non-alcoholic Steatohepatitis. *Clin Pharmacol Ther* **112**, 1271-1279 (2022). https://doi.org/10.1002/cpt.2745

44 Zhang, Y. *et al.* A new experimental rat model of nocebo-related nausea involving double mechanisms of observational learning and conditioning. *CNS Neurosci Ther* (2023). https://doi.org/10.1111/cns.14389

45 Seroogy, K. B., Fallon, J. H., Loughlin, S. E. & Leslie, F. M. Few cortical cholecystokinin immunoreactive neurons have long projections. *Exp Brain Res* **59**, 533-542 (1985). https://doi.org/10.1007/BF00261344

46 Frezel, N. *et al.* In-Depth Characterization of Layer 5 Output Neurons of the Primary Somatosensory Cortex Innervating the Mouse Dorsal Spinal Cord. *Cereb Cortex Commun* **1**, tgaa052 (2020). https://doi.org/10.1093/texcom/tgaa052

47 Millan, M. J. Descending control of pain. *Prog Neurobiol* **66**, 355-474 (2002). https://doi.org/10.1016/s0301-0082(02)00009-6

48 Calejesan, A. A., Kim, S. J. & Zhuo, M. Descending facilitatory modulation of a behavioral nociceptive response by stimulation in the adult rat anterior cingulate cortex. *Eur J Pain* **4**, 83-96 (2000). https://doi.org/10.1053/eujp.1999.0158

49 Seroogy, K. B., Fallon, J. H., Loughlin, S. E. & Leslie, F. M. Few cortical cholecystokinin immunoreactive neurons have long projections. *Exp Brain Res* **59**, 533-542 (1985). https://doi.org/10.1007/BF00261344

50 Fillinger, C., Yalcin, I., Barrot, M. & Veinante, P. Efferents of anterior cingulate areas 24a and 24b and midcingulate areas 24a' and 24b' in the mouse. *Brain Struct Funct* **223**, 1747-1778 (2018). https://doi.org/10.1007/s00429-017-1585-x

51 An, X., Bandler, R., Ongur, D. & Price, J. L. Prefrontal cortical projections to longitudinal columns in the midbrain periaqueductal gray in macaque monkeys. *J Comp Neurol* **401**, 455-479 (1998).

52 Lee, J. Y. *et al.* Role of anterior cingulate cortex inputs to periaqueductal gray for pain avoidance. *Current biology : CB* **32**, 2834-2847 e2835 (2022). https://doi.org/10.1016/j.cub.2022.04.090

53 Xiao, X. & Zhang, Y. Q. A new perspective on the anterior cingulate cortex and affective pain. *Neurosci Biobehav Rev* **90**, 200-211 (2018). https://doi.org/10.1016/j.neubiorev.2018.03.022

54 Levine, J. D., Gordon, N. C. & Fields, H. L. The mechanism of placebo analgesia. *Lancet* **2**, 654-657 (1978). https://doi.org/10.1016/s0140-6736(78)92762-9

55 Benedetti, F., Amanzio, M. & Thoen, W. Disruption of opioid-induced placebo responses by activation of cholecystokinin type-2 receptors. *Psychopharmacology (Berl)* **213**, 791-797 (2011). https://doi.org/10.1007/s00213-010-2037-y

56 Seymour, B. Pain: A Precision Signal for Reinforcement Learning and Control. *Neuron* **101**, 1029-1041 (2019). https://doi.org/10.1016/j.neuron.2019.01.055

57 Krahe, C., Springer, A., Weinman, J. A. & Fotopoulou, A. The social modulation of pain: others as predictive signals of salience - a systematic review. *Front Hum Neurosci* **7**, 386 (2013). https://doi.org/10.3389/fnhum.2013.00386

58 Colloca, L. & Finniss, D. Nocebo effects, patient-clinician communication, and therapeutic outcomes. *Jama* **307**, 567-568 (2012). https://doi.org/10.1001/jama.2012.115

59 Corsi, N. & Colloca, L. Placebo and Nocebo Effects: The Advantage of Measuring Expectations and Psychological Factors. *Front Psychol* **8**, 308 (2017). https://doi.org/10.3389/fpsyg.2017.00308

60 Manai, M., van Middendorp, H., Veldhuijzen, D. S., Huizinga, T. W. J. & Evers, A. W. M. How to prevent, minimize, or extinguish nocebo effects in pain: a narrative review on mechanisms, predictors, and interventions. *Pain Rep* **4**, e699 (2019). https://doi.org/10.1097/PR9.0000000000000699

61 Sorge, R. E. *et al.* Olfactory exposure to males, including men, causes stress and related analgesia in rodents. *Nat Methods* **11**, 629-632 (2014). https://doi.org/10.1038/nmeth.2935

62 Cowie, A. M. & Stucky, C. L. A Mouse Model of Postoperative Pain. *Bio Protoc* **9** (2019). https://doi.org/10.21769/BioProtoc.3140

63 Xu, J. & Brennan, T. J. Comparison of skin incision vs. skin plus deep tissue incision on ongoing pain and spontaneous activity in dorsal horn neurons. *Pain* **144**, 329-339 (2009). https://doi.org/10.1016/j.pain.2009.05.019

64 Bennett, G. J. & Xie, Y. K. A peripheral mononeuropathy in rat that produces disorders of pain sensation like those seen in man. *Pain* **33**, 87-107 (1988).

65 Zumbusch, A. S., McEachern, E. L. F., Morgan, O. B., Nickner, E. & Mogil, J. S. Normative Preclinical Algesiometry Data on the von Frey and Radiant Heat Paw-Withdrawal Tests: An Analysis of Data from More Than 8,000 Mice Over 20 Years. *J Pain* **25**, 104468 (2024). https://doi.org/10.1016/j.jpain.2024.01.333

66 Li, C. L. *et al.* Validating Rat Model of Empathy for Pain: Effects of Pain Expressions in Social Partners. *Front Behav Neurosci* **12**, 242 (2018). https://doi.org/10.3389/fnbeh.2018.00242

67 Laviola, G. *et al.* Low empathy-like behaviour in male mice associates with impaired sociability, emotional memory, physiological stress reactivity and variations in neurobiological regulations. *PloS one* **12**, e0188907 (2017). https://doi.org/10.1371/journal.pone.0188907

68 Smith, M. L., Asada, N. & Malenka, R. C. Anterior cingulate inputs to nucleus accumbens control the social transfer of pain and analgesia. *Science* **371**, 153-159 (2021). https://doi.org/10.1126/science.abe3040

69 Hargreaves, K., Dubner, R., Brown, F., Flores, C. & Joris, J. A new and sensitive method for measuring thermal nociception in cutaneous hyperalgesia. *Pain* **32**, 77-88 (1988). https://doi.org/10.1016/0304-3959(88)90026-7

70 Chaplan, S. R., Bach, F. W., Pogrel, J. W., Chung, J. M. & Yaksh, T. L. Quantitative assessment of tactile allodynia in the rat paw. *J Neurosci Methods* **53**, 55-63 (1994).

71 Rosland, J. H., Tjølsen, A., Mæhle, B. & Hole, K. The formalin test in mice: effect of formalin concentration. *Pain* **42**, 235-242 (1990). https://doi.org/10.1016/0304-3959(90)91167-h

72 Chesler, E. J. *et al.* Genotype-dependence of gabapentin and pregabalin sensitivity: the pharmacogenetic mediation of analgesia is specific to the type of pain being inhibited. *Pain* **106**, 325-335 (2003). https://doi.org/10.1016/s0304-3959(03)00330-0

73 Coderre, T. J., Fundytus, M. E., McKenna, J. E., Dalal, S. & Melzack, R. The formalin test: a validation of the weighted-scores method of behavioural pain rating. *Pain* **54**, 43-50 (1993). https://doi.org/10.1016/0304-3959(93)90098-a

74 Fischer, M., Carli, G., Raboisson, P. & Reeh, P. The interphase of the formalin test. *Pain* **155**, 511-521 (2014). https://doi.org/10.1016/j.pain.2013.11.015

75 Friard, O. & Gamba, M. BORIS: a free, versatile open-source event-logging software for video/audio coding and live observations. *Methods in Ecology and Evolution* **7**, 1325-1330 (2016). https://doi.org/10.1111/2041-210X.12584

76 Bankhead, P. *et al.* QuPath: Open source software for digital pathology image analysis. *Sci Rep* **7**, 16878 (2017). https://doi.org/10.1038/s41598-017-17204-5

77 Keay, K. & Bandler, R. in *The Senses: A Comprehensive Reference* (eds Richard H. Masland *et al.*) 627-634 (Academic Press, 2008).

Figure Legends

Fig. 1. Contextual and social nocebo pain behavior in mice depends on cholecystokinin receptors. (**A**) Timeline of contextual conditioning when hind paw incision is used as the unconditioned stimulus (UCS). (**B – E**) Mechanical pain sensitivity of mice of both sexes combined on days 1 and 6 in the same context (**B**), in a different context (**C**), in the same context following treatment with proglumide (**D**), and in the same context following treatment with LY225910 (**E**) when hind paw incision is used as the UCS. (**F**) Timeline of the social nocebo procedure. (**G**) Chemical sensitivity in mice following the social nocebo procedure as assessed by the formalin assay. (**H**) Time course of mechanical sensitivity at 0, 4, and 24 h after the social nocebo in No Pain Observer (i.e., mice that did not socially interact with a cagemate in pain), Pain Observer mice, and Pain Observer mice treated with proglumide (n = 10 – 12 mice/group). The data for box plots show the interquartile range (IQR), with the box representing Q1 to Q3, the line denoting Q2 (median), and the whiskers extending between the minimum and maximum values. The dots represent individual data points, shown as before and after plots for the contextual (conditioning) nocebo data (B–E). Symbols in panel H represent mean ± SEM for mechanical withdrawal threshold (g). Statistical tests include one-way ANOVA for hind paw incision (panels B–E) and chemical sensitivity (panel G); two-way mixed ANOVA (condition X day) for mechanical sensitivity (panel H). $*p < 0.05$, $**p < 0.01$, $***p < 0.001$ representative of post hoc comparisons using paired *t*-tests with Bonferroni correction. All statistical measure details are shown in file S1.

Fig. 2. Activation of distinct regions of the periaqueductal gray by contextual and social nocebo pain. Timeline of contextual nocebo (**A**) and social nocebo (**B**) pain models to capture activated neurons by c-Fos staining. (**C**) Illustrations showing the regions of the periaqueductal gray (PAG) and bregma coordinates for c-Fos quantification (aPAG, anterior PAG; imPAG, intermediate PAG; pPAG, posterior PAG). (**D**) Number of c-Fos-positive cells in the aPAG for contextual and social nocebo pain models. (**E**) Number of c-Fos-positive cells in the imPAG for contextual and social nocebo pain models. (**F**) Number of c-Fos-positive cells in the pPAG for contextual and social nocebo pain models. (**G**) Representative photomicrographs of the imPAG for contextual nocebo groups. Scale bars indicate 200 µm for a 10X image and 50 µm for a zoomed image. (**H**) Representative photomicrographs of the imPAG for social nocebo groups. Scale bars indicate 160 µm for a 4X image and 30 µm for a zoomed image. Box plots show the interquartile range (IQR), with the box representing Q1 to Q3, the line denoting Q2 (median), and the whiskers extending between the minimum and maximum values. The dots represent individual data points, representing the average c-Fos counts per mm^2 across three sections per mouse per bregma coordinate. Columns of PAG quantification include dorsomedial, dorsolateral, lateral PAG, and ventrolateral (dmPAG, dlPAG, lPAG, and vlPAG, respectively). One-way ANOVA with Holm-Sidak post hoc tests comparing conditions across each region, $*p < 0.05$, $**p < 0.01$, $***p < 0.001$. All statistical measure details are presented in file S1.

Figure 3. Activation of cholecystokinin receptors in the lateral (but not dorsomedial) periaqueductal gray is necessary for nocebo-induced pain and sufficient to elicit pain behavior. (**A**) Illustration and representative micrograph for cannulation and microinjection of the intermediate dorsomedial PAG (dmPAG). For the representative section, fluorescently labeled muscimol (250 nl per side over 5 min) allowed the visualization of injection spread. Scale bar indicates 100 µm. (**B**) von Frey data for contextual nocebo (hind paw incision) before and after re-exposure to the same context, with aCSF or proglumide infusion in the intermediate dmPAG. (**C**)

Electronic von Frey data for social nocebo before and following 'pain observation', with aCSF or proglumide infusion in the intermediate dmPAG. (**D**) CCK-8S infusion in the intermediate dmPAG does not change mechanical thresholds on the electronic von Frey test. (**E**) CCK-8S infusion in the intermediate dmPAG does not alter thermal responses on the hot plate. (**F**) Illustration and representative micrograph for cannulation and microinjection of the intermediate lateral PAG (lPAG). For the representative section, fluorescently labeled muscimol (250 nl per side over 5 min) allowed the visualization of injection spread. Scale bar indicates 500 µm. (**G)** von Frey data for contextual nocebo (hind paw incision) before and after re-exposure to the same context, with aCSF or proglumide infusion in the intermediate lPAG. (**H**) Electronic von Frey data for social nocebo before and following 'pain observation,' with aCSF or proglumide infusion in the intermediate lPAG. (**I**) CCK-8S infusion in the intermediate lPAG increases mechanical sensitivity on the electronic von Frey test. (**J**) CCK-8S infusion in the intermediate lPAG decreases latency to lick on the hot plate. (**K**) Representative RNAscope images for identifying activated neurons (*Fos*) that contain *Cckbr* mRNA in the intermediate lPAG for contextual nocebo. Scale bar indicates 100 µm. (**L**) Violin plots showing quantification of $Cckbr^+$ and Fos^+ neurons in the intermediate lPAG of mice placed in the same or different context. (**M**) Representative RNAscope images for identifying activated neurons (*Fos*) that contain *Cckbr* mRNA in the intermediate lPAG for social nocebo. Scale bar indicates 100 µm. (**N**) Violin plots showing quantification of $Cckbr^+$ and Fos^+ neurons in the intermediate lPAG of No Pain Observers or Pain Observers. Box plots show the interquartile range (IQR), with the box representing Q1 to Q3, the line denoting Q2 (median), and the whiskers extending between the minimum and maximum values. The dots represent individual data points, shown as before and after plots for the contextual (B and G) and social (C and H) nocebo data. Separate two-way mixed ANOVAs (drug X RM) for the dmPAG and lPAG for contextual (B and G) and social nocebo (C and H); two-way mixed ANOVA (drug X RM) for mechanical sensitivity (D and I); paired t-tests for hot-plate data (E and J). $*p < 0.05$, $**p < 0.01$, $***p < 0.001$ representative of post hoc comparisons using the Holm-Sidak test or t-test significance. All statistical measure details are shown in file S1.

Figure 4. Cholecystokinin neurons in the ACC project to the intermediate lPAG and are necessary for nocebo-induced pain hypersensitivity and sufficient to trigger pain hypersensitivity. (**A**) Illustration of a Cre-dependent retrograde virus injection (rAAV-CAG-DIO-mNeptune) into the intermediate lateral periaqueductal gray (lPAG) of CCK-Cre mice and identification of viral expression across candidate brain regions (**B**) A set of micrographs is shown that portray retrograde tracing of CCK^+ neurons from the intermediate lPAG. Sections demonstrate many CCK^+ neurons in the anterior cingulate cortex (ACC) and fewer such cells in subsections of the insular, motor, retrosplenial, and parietal cortices. There is also a small cluster of cells in the auditory cortex. (**C-E**) Magnified micrographs from the same tracing in (B) Scale bar indicates 200 µm. (**C**) Micrograph displaying co-expression of the retrograde viral tracer with the neuronal marker, NeuN in the injection site: intermediate lPAG. (**D**) Micrographs showing co-expression of the retrograde viral tracer with NeuN in the insular, motor, retrosplenial, and parietal cortices. (**E**) Micrograph displaying co-expression of the retrograde viral tracer with the neuronal marker, NeuN in the ACC. In panels D and E, all NeuN neurons and NeuN neurons with CCK co-expression were counted within layer V (red outline) of the respective cortical areas. (**F**) Violin plots showing the percentage of CCK^+ neurons relative to the total NeuN staining in the regions of interest. (**G**) Schematic and timeline showing Cre-dependent eOPN3 or control virus injection in the ACC with optical fiber implant in the intermediate lPAG followed by contextual or social

nocebo pain behavior. **(H)** Mechanical sensitivity data from contextual nocebo (hind paw incision) with inhibition of ACC→lPAG projections in mCherry- and eOPN3-mice before (BL) and following re-exposure to the same context (Light On). (**I**) Mechanical sensitivity data from social nocebo with inhibition of ACC→lPAG projections in mCherry- and eOPN3-mice before (BL) and following social interaction with a pain demonstrator (Light On). (**J**) Schematic and timeline showing Cre-dependent ChR2 or control virus injection in the ACC with optical fiber implant in the intermediate lPAG followed by mechanical sensitivity test using the von Frey test. (**K**) Activation of CCK^+ ACC→lPAG projections by ChR2 increases pain behavior on the von Frey test. Box plots show the interquartile range (IQR), with the box representing Q1 to Q3, the line denoting Q2 (median), and the whiskers extending between the minimum and maximum values. The dots represent individual data points, which are shown as before and after plots for contextual nocebo (**H**), social nocebo (**I**), and ChR2 **(K)** data. One-way ANOVA (F, K) or two-way mixed ANOVA (virus X RM) for nocebo behavioral tests (H and I). $*p < 0.05$, $*p < 0.01$, $***p < 0.001$ representative of post hoc comparisons using the Holm-Sidak test. All statistical measure details are shown in file S1.

Materials and Methods

Experimental animals

Most experiments used naive, adult CD-1 (ICR:Crl) or C57BL/6 mice aged 6–13 weeks, of both sexes. CD-1 mice were bred in-house at McGill University, originating from breeders obtained from Charles River (St. Constant, QC). C57BL/6 mice were purchased from Charles River (St. Constant, QC) and housed in the University of Toronto Mississauga (UTM) vivarium for at least two weeks prior to starting behavioral testing. Experiments targeting CCK neurons used offspring bred in-house (UTM) from CCK-IRES-Cre mice, which were originally purchased from The Jackson Laboratory (Bar Harbor, ME; Stock #012706). All mice were group-housed in cages of 2–4 on individually ventilated cage racks (Techniplast North America) in a temperature-controlled (22 ± 2°C) room with access to food (Harlan Teklad 8604 for McGill mice; 2019 Teklad for UTM mice) and water *ad libitum*. Both vivaria were maintained under a temperature-controlled environment and operated on a 12:12 h light/dark cycle (lights on at 07:00 h). Mice were allocated randomly to experimental groups and testing was conducted by multiple female experimenters[61] who were blind to drug treatments. All procedures adhered strictly to Canadian Council on Animal Care regulations and received approval from local animal care and use committees.

Pharmacological agents

Proglumide (10 mg/kg; Tocris or Sigma Aldrich) was dissolved in saline and administered intraperitoneally (i.p.). LY225910, the CCK-2 antagonist (1 mg/kg, Tocris) was dissolved in 5% DMSO in saline using a sonicator or 5% DMSO and 0.5% Tween-80 in saline and administered intraperitoneally (i.p.). Loxiglumide, the CCK-1 antagonist (10 mg/kg, Tocris) was dissolved in saline and administered i.p. Metyrapone (50 mg/kg, Sigma Aldrich) was dissolved in saline and administered subcutaneously (s.c.) after a 1 h habituation at the start of the social nocebo procedure. Systemically administered drugs were injected using a volume of 10 ml/kg body weight. In microinfusion experiments, proglumide (250 ng in 250 nl aCSF, Sigma Aldrich) or CCK-sulfated octapeptide (CCK-8S) (50 ng in 250 nl aCSF, Cayman Chemicals) were microinfused through implanted cannulas via calibrated tubing (see below).

Viral reagents

Viruses were injected at a volume of 200 nl for functional experiments and 100 nl for tracing. AAVretro-CAG-DIO-mNeptune, AAV2/9-hSYN1-SIO-eOPN3-mScarlet, AAV2/9-EF1α -DIO-ChR2(H134R)-mCherry, and AAV2/9-EF1α-DIO-mCherry were purchased from Neurophotonics (Quebec City, QC). AAV2/8-hSYN-DIO-mCherry, and AAV-2/8-CamkIIa-GFP were purchased from Addgene (Watertown, MA).

Pain hypersensitivity conditioning paradigms (Contextual nocebo)

The conditioning paradigms comprised three distinct phases: baseline testing where basal thresholds were measured, the learning session, during which the association between pain (unconditioned stimulus, UCS) and context (conditioned stimulus, CS) was formed, and the testing day, which assessed the response to the presentation of the CS. Two different pain stimuli were used as the UCSs: hind paw incision, or chronic constriction injury, as described below.

Prior to surgery, mechanical thresholds were assessed using the von Frey test (see below). On the learning day, mice underwent either hind paw incision surgery on their left paw to induce post-surgical pain, or CCI on their left leg, which served as the UCSs. Following surgery, while still

under anesthesia, the mice were placed in the conditioning context, consisting of Plexiglas cubicles within a specific laboratory testing room, where they remained for 5 hours, most of which was spent awake. Mice subjected to incision and CCI surgery were returned to the same or different context at 6 or 14 days after surgery, respectively. On test days, mice were retested for pain sensitivity following a 10–90-min habituation period using the manual von Frey test. For baseline and test day measurements, four separate determinations, two per hind paw, were conducted and averaged. In some experiments, mice received an i.p. injection of proglumide (10 mg/kg) prior to placement in the context on test day or LY-225910 (1 mg/kg) before the surgery and 30 min prior to testing on the test day.

Hind paw incision surgery

The hind paw incision surgery was done following the protocol of Cowie and Stucky [62]. Mice were anesthetized by continuous inhalation of isoflurane. A 5-mm incision through the skin and facia was performed on the left hind paw of the mouse. The flexor digitorum brevis muscle was elevated with forceps or blunt dissection probe and a longitudinal incision was made through the muscle by a scalpel. The wound was closed with two skin sutures. This assay mimics invasive surgery and causes acute pain and hypersensitivity that lasts up to two weeks [63].

CCI surgery. The CCI was performed following the procedure of Bennett and Xie [64]. The sciatic nerve was exposed midway along the thigh using gentle dissection through the biceps femoris muscle. Preceding the trifurcation of the sciatic nerve, approximately 7 mm of nerve tissue was released from surrounding adhesions. Three ligatures (7-0 silicone coated braided silk, Sofsilk) were loosely tied around the nerve, spaced roughly 1 mm apart. The affected nerve segment measured between 4–5 mm in length. Particular attention was paid to tying the ligatures to ensure minimal constriction of the nerve when examined under 40x magnification. The intended level of constriction impeded, but did not fully halt, circulation through the outer blood vessels of the nerve, occasionally eliciting a brief muscle twitch around the exposed area. The incision was subsequently closed in layers. This assay mimics neuropathic pain states in humans, and in our hands causes hypersensitivity lasting more than a month [65].

One-in-pain social interaction (Social nocebo)

Same sex cagemate pairs were placed in an open top/bottom box (inner dimensions: 14.5 cm x 14.5 cm x 30 cm) with three opaque sides and one clear side. Each box was set on top of a clear acrylic platform, which was either placed on a frame for the formalin assay to record video from below or set on top of a lab bench for all other assays. For each experiment, pairs of mice were habituated to the box for 1 h. Mice in the pair were randomly assigned as either observer or demonstrator. Following habituation, the demonstrator was removed briefly, administered an intraplantar hind paw injection of formalin (2.5%, 20 µl; Pain Observer condition), or 0.09% saline as a no-pain control stimulus (No Pain Observer condition). Formalin hind paw injection was selected as the pain stimulus for the Pain Observer condition due to the characteristic pattern of overt nocifensive behaviors that are reliably perceived by observer mice [66,67]. The observer and demonstrator were then allowed to interact for 30 min, a duration selected based on previously published social transfer/emotional contagion models [19,66-68]. Following the 30 min one-in-pain social interaction, the demonstrator was removed from the box and returned to its home cage. The observer was then either tested for formalin sensitivity (20 µl, 0.5%) intraplantar to the left hind paw or placed in individual Plexiglas cubicles over a metal mesh platform for electronic von Frey testing (see below). For von Frey testing, baseline measurements consisted of five separate determinations for each hind paw, which were averaged. The observer and demonstrator

underwent the social nocebo procedure, after which the observer was tested for mechanical sensitivity. In one experiment, mice were tested immediately after, 4 h after, and 24 h after the one-in-pain social interaction. However, most von Frey experiments for the social nocebo paradigm report the average of two measurements per paw starting at 10 min after placing the observer into the Plexiglas cubicle.

Quantification of social behavior

In a subset of mice, behaviors during the 30-min one-in-pain social interaction were counted. Behaviors were sampled during the first 10 s of every minute. Data were quantified as the percent positive samples across the 30-min session. In the demonstrator mouse we recorded hind paw licking. In the observer mouse we recorded: (1) attending toward the cagemate including sniffing or grooming, excluding the anogenital region, and (2) propinquity behavior defined as being within 2 cm or less of the demonstrator mouse, but not actively engaging in attending behavior.

Pain behavior tests

Radiant heat paw-withdrawal test

The Hargreaves' radiant heat paw-withdrawal test was used to assess acute thermal nociception sensitivity in mice [69]. Prior to behavioral testing, mice were individually housed in perforated, transparent Plexiglas enclosures (5 cm by 8.5 cm by 6 cm) situated on a glass floor with a thickness of 3/16th inches and allowed to acclimate for 2 h. A high-intensity beam (IITC model 336; ≈ 45 W) emitted from a projector lamp bulb positioned 6 cm beneath the glass floor was directed at the plantar surface of the mid-hind paw of each mouse at rest. Withdrawal latency of each hind paw was recorded to the nearest 0.1 s. For the acetic acid UCS experiments, reported latencies represent the average of eight separate measurements.

von Frey test

Testing of mechanical sensitivity was performed using either the manual or electronic von Frey test, depending on the laboratory where the experiment was performed. *Manual von Frey:* In contextual nocebo experiments, mice were placed individually in transparent Plexiglas cubicles (5 cm x 8.5 cm x 6 cm) on top of a perforated metal floor and habituated for 2 h before testing. Nylon monofilaments (force range: ≈0.015 to 1.3 g; Touch Test Sensory Evaluator Kit, Stoelting) were firmly applied to the plantar surface of each hind paw of an inactive mouse until they bowed for 0.5 s. The up-down method of Dixon [70] was used to estimate 50% withdrawal thresholds. *Electronic von Frey:* In social nocebo and cannulation experiments, observers were placed in individual Plexiglas cubicles (10 cm x 5.5 cm x 6.5 cm) over a metal mesh platform and allowed to habituate for 30 min prior to baseline testing. Mice were tested using a Dynamic Plantar Aesthesiometer (Ugo Basile, 37450, Gemonia, Italy) which raised a blunt 0.5-mm metal probe onto the center of the hind paw and gradually applied force (0–10 g ramp over 10 s) until the mouse withdrew its hind paw. The maximal pressure displayed upon withdrawal was recorded.

Formalin test

In social nocebo experiments, a low concentration of formalin (0.5%, 20 µl) administered intraplantar to the left hind paw was used to measure chemical pain sensitivity in observer mice. This concentration was chosen because it typically elicits minimal nocifensive behavior and avoids a behavioral ceiling effect [71]. The observer mouse was returned to the box after paw injection and behaviors were digitally recorded for 60 min. Afterward, videos were sample scored across the first 10 s of every minute where the presence of licking/biting of the left hind paw was recorded for a total of 60 observations [72]. Formalin hind paw injection typically presents a pattern of

vigorous licking in the first 5–10 min deemed the "early phase", a quiescent period in the next 5–10 min where very little licking occurs, then a "late phase" of sporadic licking that occurs throughout the remainder of the testing period [73,74]. Formalin data presented throughout the paper represent the percent positive samples across the late phase of the test.

Hot-plate thermal sensitivity test

The hot-plate test was used to assess whether applying CCK to the dmPAG or lPAG enhanced thermal sensitivity. Mice were tested in a counterbalanced manner on the hot plate 30 min after microinfusion with CCK or aCSF, then 48 h later were retested with the other drug. After microinfusion, mice were immediately moved to the testing room. Mice were then placed singly on a clean hot plate set at 52.5 °C for 45 s. Videos were analyzed using BORIS (Behavioral Observation Research Interactive Software) [75] for the cumulative number of hind paw flicks and the latency to first hind paw flick, lick, or jump.

Additional behavioral tests

Elevated plus maze

The maze consisted of a white acrylic plus-shaped platform elevated 50 cm from the floor, with two closed arms, two open arms, and an open center. Mice were placed in the center of the plus maze facing the open arms and left to freely roam for 5 min. Behavior was recorded from above and manually coded for number of open and closed arm entries and time spent in open or closed arms using BORIS [75]. An open arm entry was strictly defined as crossing outside of the center zone into the open arm by both fore paws and snout, while a closed arm entry was defined as crossing out of the center zone into the closed arm with both fore paws and snout. The time in the center zone was excluded from data analysis. The maze was cleaned with ethanol between each animal.

Open field

Mice were placed in the center of a white open field box (42 cm x 42 cm x 42 cm) and recorded for 10 min (EthoVision XT v.11.5, Noldus Information Technology, Leesburg VA). Total distance traveled and velocity data were collected as measures of the effect of proglumide in the lPAG on motor response because systemically administered proglumide and CCKergic drugs have been shown to influence motor behavior [28]. Mice were tested without infusion (Day 1), 48 h later with proglumide infusion (Day 2), and again 48 h later without infusion (Day 3) in the open field for potential changes in distance traveled or velocity. Mice were tested in the open field box 90 min after proglumide infusion to correspond with testing for mechanical sensitivity after 1 h habituation and 30 min one-in-pain social interaction.

Stereotaxic surgery and related manipulations

All surgeries were performed under sterile conditions. Mice were anesthetized with isoflurane (4% induction, 2–2.5% maintenance) and body heat maintained on a circulating heated water mat. The scalp was sterilized, shaved, a small incision was made in the skin, the skull leveled using a digital stereotaxic instrument (Harvard Apparatus, Holliston, MA), and burr holes drilled at the respective stereotaxic coordinates. Mice were treated with postsurgical analgesia (20 mg/kg meloxicam) once daily for three days.

Cannulations and microinfusion experiments

Mice were cannulated with either a single cannula for drug application to the dmPAG or a double cannula for bilateral drug application to the lPAG. Separate cohorts of mice for both region and

drug were used and then tested on either von Frey or hot-plate tests. A single guide cannula with length 3.0 mm and injector cut 0.5 mm below the pedestal (C315GS-5/spc, P1 Technologies, Roanoke, VA) was implanted above the dmPAG (11.7° angle, AP -3.6 mm, ML -0.2 mm, DV -2.55 mm), or a double guide cannula (RWD Life Science, San Diego, CA: guide cannula 62056, center distance 1.4 mm, length 3.0 mm, dummy 62127, injector 62056, both cut 0.5 mm below guide cannula, cap 62525) was implanted above the lPAG (AP -3.85 mm, ML ±0.55 mm, DV -2.65 mm) at 7 weeks of age. Following a 7-day recovery period, mice were tested for baseline von Frey sensitivity and then either underwent contextual nocebo or social nocebo procedures (see above). In all experiments, microinfusions were performed under light isoflurane anesthesia immediately preceding context exposure or the 1-h habituation before social nocebo. In **Fig. 3, D to I**, infusions occurred 30–45 min before pain testing. During infusion, calibrated tubing was used to connect the internal cannula to a microliter syringe (1700 series Hamilton Syringe, 100 µl, Harvard Apparatus, Montreal QC) and an infusion pump (Pump 11 Elite Nanomite, Harvard Apparatus, Montreal QC) was used to infuse a 0.25-µl volume over 5 min (50 nl/min), after which the injector was left in place for an additional 1 min. Mice were allowed to recover in their home cage prior to testing. Cannula placement was later verified through infusion of 250 nl of muscimol-BODIPY (M23400, Invitrogen). Mice with placement outside of the target region (dmPAG or lPAG) were excluded (< 5%).

Viral infusions

Viruses were infused at a rate of 60 nl/min using a glass capillary micropipette backfilled with mineral oil and attached to a 1700 series gas-tight Hamilton microsyringe. Micropipettes were lowered 0.1 mm below injection site (ACC: AP +1.0 mm, ML ±0.5 mm, DV -0.8 mm; lPAG: AP -3.85 mm, ML ±0.5 mm, DV -2.65 mm) prior to infusion and left in position for 10 min prior to slow removal to prevent backflow. Skin was sutured and the mouse recovered on a heated pad. Viruses were allowed three weeks of expression prior to behavioral testing or tracing.

Optogenetic manipulations

CCK-IRES-Cre mice were infused with virus expressing eOPN3, ChR2, or control in the lPAG. In the same surgery session, an optic fiber cannula (200 µm core, 3.0 mm length, R-FOC-BL200C-39NA, RWD Life Science, San Diego, CA) was implanted above the lPAG and secured with dental cement (3M ESPE RelyX Unicem Aplicap Self-Adhesive Universal Resin Cement, 56818). The virus was allowed to express for three weeks. <u>*Contextual nocebo:*</u> For the hind paw incision eOPN3 experiment, viruses were injected 2 weeks prior to baseline, followed by hind paw incision surgery and conditioning to the cubicles. This allowed the virus to express for a total of 3 weeks before mice were tested on test day. In addition, mice were connected to the patch cord (200 nm, Doric, Quebec City, QC) for 10 min at the beginning of the 5 h conditioning period in the contextual nocebo experiments. Then, on the test day mice were tethered and immediately put into the observation box, exposed to that box for 30 min, then put into the von Frey cubicle and allowed to rest for 10 min. They were then tested for mechanical sensitivity using the manual von Frey test. <u>*Social nocebo:*</u> Two days prior to testing in the social nocebo paradigm, pairs were habituated to the box for 1 h. One day prior to testing, pairs were habituated again to the box for 30 min, then the observer mouse was habituated to the patch cord in the box for 10 min. On test day, pairs were habituated for 1 h to the container, then the patch cord was attached to the observer mouse that was allowed to further acclimate for 5 min. <u>*Optical Stimulation for eOPN3:*</u> Light delivery was initiated immediately after placement in the conditioning box for contextual nocebo or following formalin injection in the demonstrator for social nocebo. Optical stimulation consisted of 50 ms

pulses at a light power density of 10 mW/mm^2 of 470 nm light (470 nm, 50 W Collimated LED BLS-LCS-0470-50-22, Oasis Implant, Polyscan3 software, Mightex, Toronto, Canada) delivered once every 2 min to the lPAG of the conditioned mouse or observer for the 30 min duration. Mice were then moved to individual Plexiglas cubicles over a metal mesh platform and tested for mechanical sensitivity. Values reported are the average of two measures on each hind paw. *Optical Stimulation for ChR2:* Mice were tested for baseline mechanical sensitivity. Mice were then habituated to the stimulation box for 30 min during two consecutive days prior to testing with 10 min of habituation to the patch cord each day. On test day, mice were habituated to the box with patch cord for 10 min prior to stimulation. For optogenetic photostimulation of ChR2, light output was 10 mW/mm^2 delivered at cycles of 5 ms bursts of light on and 45 ms of light off for a frequency stimulation of 20 Hz over a 3 min period. Mice were immediately removed from the stimulation box and placed in von Frey cubicles. In one experiment, mice were tested using manual von Frey and values reported represent the average of two measures on the left hind paw. In another experiment, mice were tested using electronic von Frey with the baseline representing the average of three measures and then subsequent time points (5, 15, 30, 45, 60, 90, and 120 minutes post-stimulation) are a single measure per hind paw.

Histological procedures, imaging and cell counting

Mice were deeply anesthetized with sodium pentobarbital (100 mg/kg, i.p.) and underwent transcardiac perfusion with 0.1 M phosphate-buffered saline (PBS, pH = 7.4) followed by 4% (w/v) paraformaldehyde in PBS (PFA). Brain tissue was extracted and post-fixed for 24 h in 4% PFA, then cryoprotected for 48 h in 30% (w/v) sucrose. Tissue was embedded in cutting medium (Tissue-Plus O.C.T. Compound, Fisher Scientific Canada) and frozen. Frozen tissue was then sectioned coronally on a cryostat (Cryostar NX50, ThermoFisher Scientific) at 40-µm thickness, then collected in cryoprotectant (30% w/v sucrose, 30% v/v ethylene glycol, 0.1 M PBS) until use.

Immunohistochemistry

Sections were thawed, placed in a 12-well plate, then washed three times for 5 min in 0.1 M PBS (pH = 7.4). Sections were blocked (5% normal goat serum, 0.3% Triton X-100, 0.1 M PBS) for 2 h at room temperature (RT). The block was removed, and sections were then incubated in primary antibody at 4°C. For c-Fos studies, a rabbit monoclonal antibody (rabbit α c-Fos 1:10,000 for 48 h, Synaptic Systems 226008, Göttingen, Germany) was used. In the retrograde tracing experiment, a monoclonal NeuN antibody (1:2,000 overnight, EMD Millipore MABN140, Darmstadt, Germany) or a polyclonal EMX1 antibody (1:50 overnight, Invitrogen, PA5-35373, Carlsbad, CA), were used as general or excitatory neuronal markers, respectively. Following primary antibody incubation, sections were washed three times for 5 min in PBS, then incubated with secondary antibody (*c-Fos experiments*: goat anti-rabbit, 1:500, 2 h at RT, Vector Laboratories DI-1649-1.5, Newark, CA; *NeuN and EMX1 experiments:* goat anti-rabbit Alexa Fluor 488, 1:500, 2 h at RT, Invitrogen A11008, Waltham, MA). Sections were then washed three times for 5 min in PBS, mounted on Superfrost slides and dipped in DAPI solution (1:50,000 in 0.1 M PBS, 5 min, D9542, Sigma Aldrich Canada, Oakville, ON) and coverslipped with mounting medium (Fluoromount-G, SouthernBiotech, Birmingham, AL).

Imaging and analysis of c-Fos

Digital images of coronal brain sections were taken at 4X (1.6125 µm/pixel, Biotek Cytation 5, Agilent, Santa Clara, CA) for the social nocebo paradigm or 10X (Olympus VS200 slide scanner, Evident Corporation, Tokyo, Japan) for the contextual nocebo paradigm using filters for both DAPI and Cy5. QuPath v0.3.2 [76] was used along with the Allen Mouse Brain Reference Atlas

Version 2 (Allen Institute for Brain Science, 2011) and schematic of the columns of the rat PAG [77] to draw regions of interest (ROI) around the anterior, intermediate, and posterior PAG. In addition, we used the DAPI channel to visualize changes in cell density that distinguish columnar organization of the PAG. c-Fos positive cells were determined as high grayscale signal, oval-shaped nuclei and counted using the QuPath cell detection feature followed by manual addition and subtraction of cells by researchers blinded to condition. c-Fos-positive regions were quantified and reported as number of cells/mm^2, and at least three sections between the bregma range were averaged for each ROI. An unbiased approach was taken such that sections from the anterior, intermediate, and posterior PAG as follows: Anterior PAG: between bregma -2.3 and -2.6. Intermediate PAG: between bregma -3.6 and - 3.9. Posterior PAG: between bregma -4.7 and -4.9. Representative images shown were taken at 10X for the conditioned paradigm (Olympus VS200 slide scanner) or 4X for the social paradigm (Cytation 5).

Retrograde tracer and NeuN/EMX1 analysis

The density of CCK-positive (tagged by virus) to NeuN/EMX1-positive cells was compared between selected brain regions (average of 3 slices per mouse from 2 mice for EMX1, average of 3 slices per mouse from 3 mice for NeuN). Digital images of coronal brain sections were taken at taken at 10X (Olympus VS200 slide scanner) using filters for DAPI, GFP (NeuN/EMX1) and mCherry (retrograde virus). QuPath was used along with the Allen Mouse Brain Reference Atlas Version 2 (Allen Institute for Brain Science, 2011) to draw regions of interest (ROI) in the ACC (AP +0.9 to +1.15, ACAd and ACAv), insula (AP +0.9 to +1.15, AId and AIv), motor cortex (AP -1.25 to -0.95, MOs and MOp), retrosplenial cortex (RSPd and RSPv combined), parietal cortex (AP -2.35 to -2.15, PTLp), and lPAG (AP -3.9 to -3.7). Quantification boundaries were drawn around layer V in each cortical region because retrogradely labeled cells were most abundant in this layer. NeuN-positive cells were determined as high grayscale signal, oval-shaped nuclei and counted using the QuPath cell detection feature followed by manual addition and subtraction of cells, whereas mCherry-positive (CCK$^+$) cells were quantified using the manual point counting feature. CCK cell density was calculated as a percentage of the mCherry-positive cells within in the ROI (mm^2) relative to the total number of NeuN-positive cells within the ROI. Density counts were averaged across three consecutive coronal slices for each ROI.

RNAscope

Tissue was collected and cut at 40 µm free-floating and then mounted on Superfrost Plus Gold slides. The RNAscope Multiplex Fluorescent V2 Assay (Advanced Cell Diagnostics (ACD), Inc., Newark, CA) was performed according to manufacturer instructions (UM 323100) using the fixed-frozen tissue sample pretreatment and RNAscope Protease III. Tissue was probed for *Cckbr* (CCK-2 receptor, ACD probe cat no. 439121) and *Fos* (ACD probe cat no. 316921) mRNA and respective 570 nm and 690 nm opal dyes (Akoya Biosciences). Slides were coverslipped with ProLong Gold mounting media (Invitrogen, Waltham, MA) and imaged within one week at 20X (Olympus VS200 slide scanner, Evident Corporation, Tokyo, Japan). We report active cells that express *Cckbr* in the social nocebo and contextual nocebo paradigms as the percent of *Fos*-positive cells (distinct 690 nm-positive ovals) that also express *Cckbr* (at least three 570 nm dots within a *Fos*-positive cell boundary).

Verification of viral injections

For verification of viral injections, sections were processed as described above. Injection location was considered accurate when expression of the virus was limited to the boundaries of the target

brain region. When visualization of the virus was not possible or spread of the virus was beyond the designated target, data were not included. This occurred in less than 5% of the injected mice.

Statistical analyses

IBM SPSS (v28, IBM Corp.) was used to perform all statistical analyses. An alpha criterion of 0.05 was adopted. One-way ANOVA, repeated measures ANOVA, or paired samples *t*-test analyses were used to compare groups in behavioral paradigms, reported respectively in Supplemental file S1 for main figure data and in the figure captions for supplemental data. In one-way ANOVA analyses, Holm-Sidak post hoc analysis was used where appropriate with correction for multiple comparisons. For box plots error bars represent the minimum and maximum data points in all cases. Prism (v9, GraphPad Software Inc.), Illustrator (v27.7, 2023, Adobe Inc.), and adaptations of templates from BioRender.com (2023) were used for graphical representations of data.

Acknowledgments:

Funding: This work was supported by the Canadian Institutes of Health Research PJT—189987 (LJM), the Natural Sciences and Engineering Research Council of Canada RGPIN-2023-05350 (LJM), and the Canada Research Chairs Program (LJM). SJP was supported by a University of Toronto Center for the Study of Pain Fellowship.

Corresponding authors: Correspondence and requests for materials should be addressed to lj.martin@utoronto.ca; jeffrey.mogil@mcgill.ca; spoulson@upenn.edu.

Author contributions: Conceptualization: SJP, JSM, LJM; Methodology: SJP, AS, LVP, WC, AM, JB, FTZ, AD, DCB, LL; Investigation: SJP, AS, LVP, WC, AM, JB, FTZ, AD, DCB, LL, LJM; Visualization: SJP, JSM, LJM; Funding acquisition: LJM; Supervision: JSM, LJM; Writing: LJM prepared the original draft with SJP, AS, and JSM contributing specific sections.

Competing interests: Authors declare that they have no competing interests.

Data and materials availability: All data needed to evaluate the conclusions in the paper are present in the paper or the supplementary materials. Supplementary Information is available for this paper.

Supplementary Materials

Figs. S1 to S10

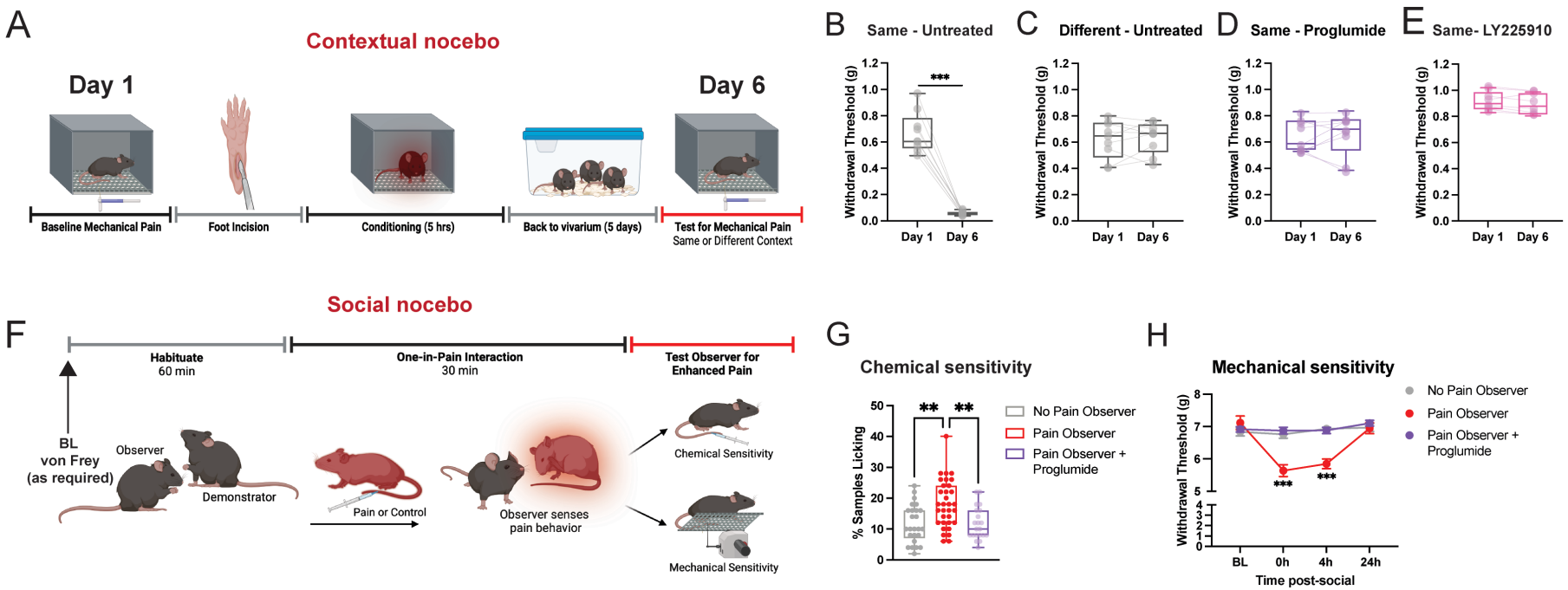
A
Contextual nocebo
Day 1
Day 6
Baseline Mechanical Pain
Foot Incision
Conditioning (5 hrs)
Back to vivarium (5 days)
Test for Mechanical Pain
Same or Different Context
B
Same - Untreated
C
Different - Untreated
D
Same - Proglumide
E
Same- LY225910
Withdrawal Threshold (g)
Day 1
Day 6
***
F
Social nocebo
Habituate
60 min
One-in-Pain Interaction
30 min
Test Observer for
Enhanced Pain
BL
von Frey
(as required)
Observer
Demonstrator
Pain or Control
Observer senses
pain behavior
Chemical Sensitivity
Mechanical Sensitivity
G
Chemical sensitivity
% Samples Licking
No Pain Observer
Pain Observer
Pain Observer +
Proglumide
H
Mechanical sensitivity
Withdrawal Threshold (g)
BL
0h
4h
24h
Time post-social

Figure 1.

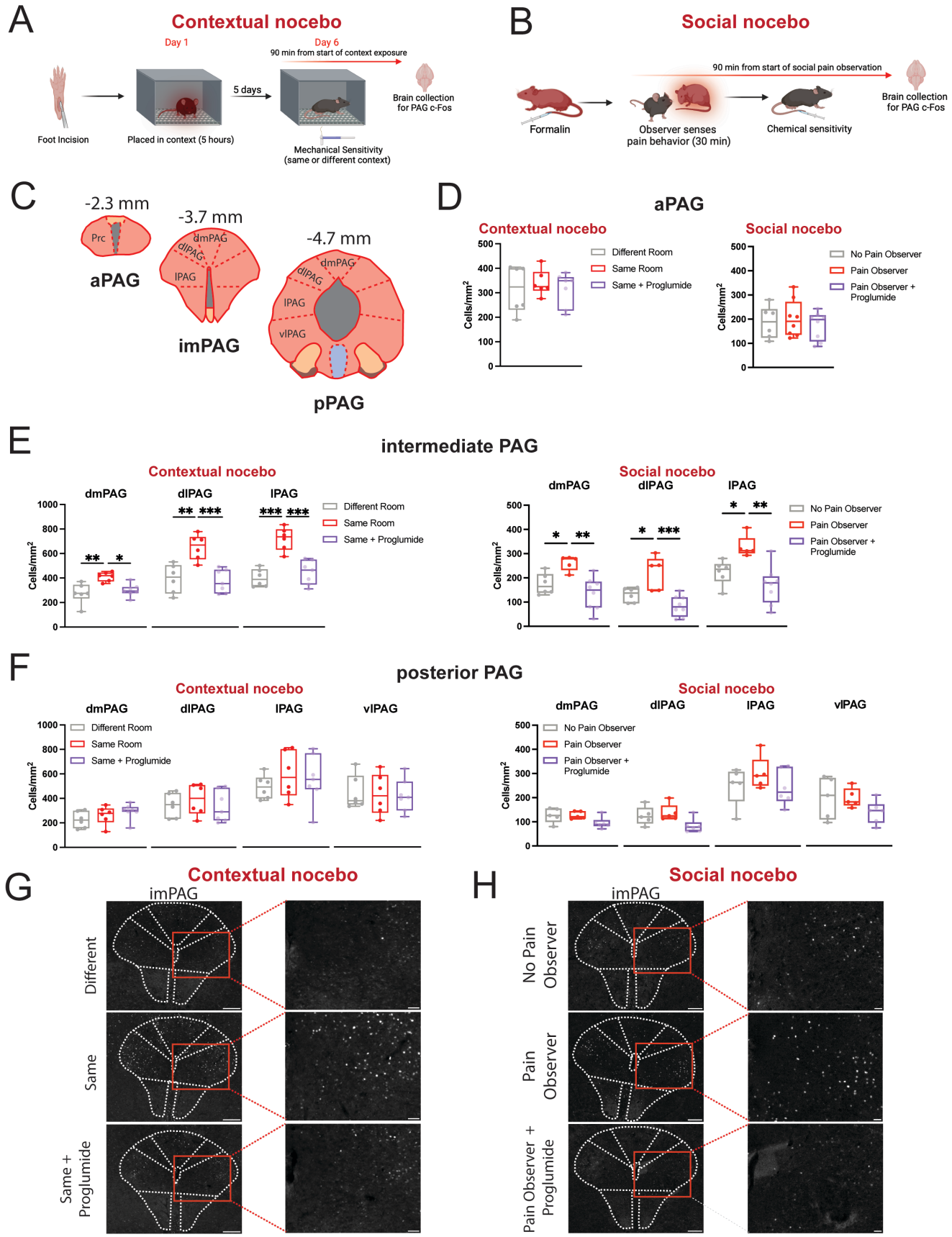
A
Contextual nocebo
Day 1
Day 6
90 min from start of context exposure
5 days
Foot Incision
Placed in context (5 hours)
Mechanical Sensitivity
(same or different context)
Brain collection
for PAG c-Fos
B
Social nocebo
90 min from start of social pain observation
Formalin
Observer senses
pain behavior (30 min)
Chemical sensitivity
Brain collection
for PAG c-Fos
C
-2.3 mm
-3.7 mm
-4.7 mm
Prc
aPAG
dmPAG
dlPAG
lPAG
imPAG
dmPAG
dlPAG
lPAG
vlPAG
pPAG
D
aPAG
Contextual nocebo
Social nocebo
Cells/mm²
Different Room
Same Room
Same + Proglumide
No Pain Observer
Pain Observer
Pain Observer +
Proglumide
E
intermediate PAG
Contextual nocebo
Social nocebo
dmPAG
dlPAG
lPAG
Cells/mm²
Different Room
Same Room
Same + Proglumide
No Pain Observer
Pain Observer
Pain Observer +
Proglumide
F
posterior PAG
Contextual nocebo
Social nocebo
dmPAG
dlPAG
lPAG
vlPAG
Cells/mm²
Different Room
Same Room
Same + Proglumide
No Pain Observer
Pain Observer
Pain Observer +
Proglumide
G
Contextual nocebo
imPAG
Different
Same
Same +
Proglumide
H
Social nocebo
imPAG
No Pain
Observer
Pain
Observer
Pain Observer +
Proglumide

Figure 2.

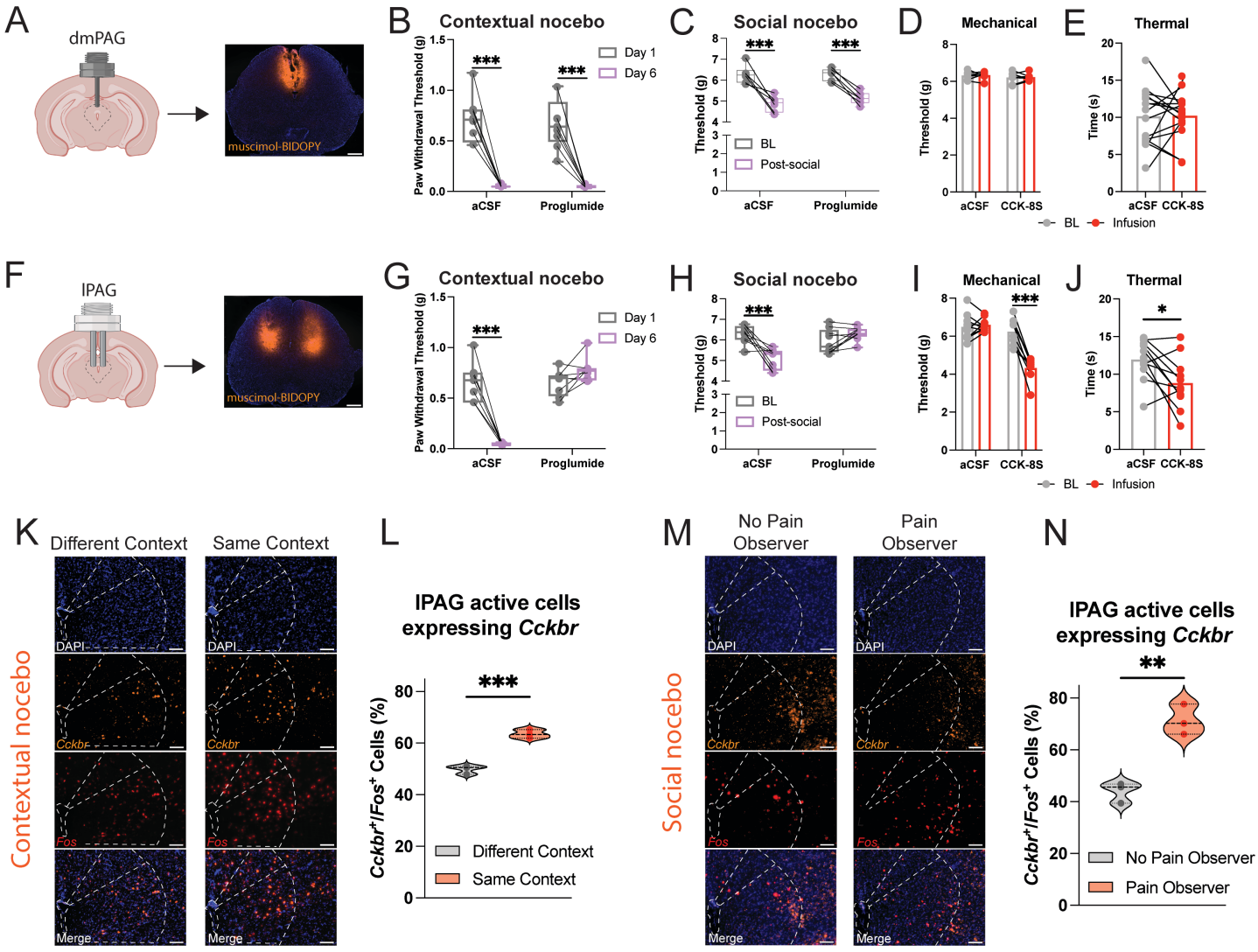
A
dmPAG
muscimol-BIDOPY
B
Contextual nocebo
Paw Withdrawal Threshold (g)
Day 1
Day 6
aCSF
Proglumide
C
Social nocebo
Threshold (g)
BL
Post-social
D
Mechanical
CCK-8S
E
Thermal
Time (s)
Infusion
F
IPAG
G
H
I
J
K
Different Context
Same Context
Contextual nocebo
DAPI
Cckbr
Fos
Merge
L
IPAG active cells expressing Cckbr
Cckbr+/Fos+ Cells (%)
M
No Pain Observer
Pain Observer
Social nocebo
N

Figure 3.

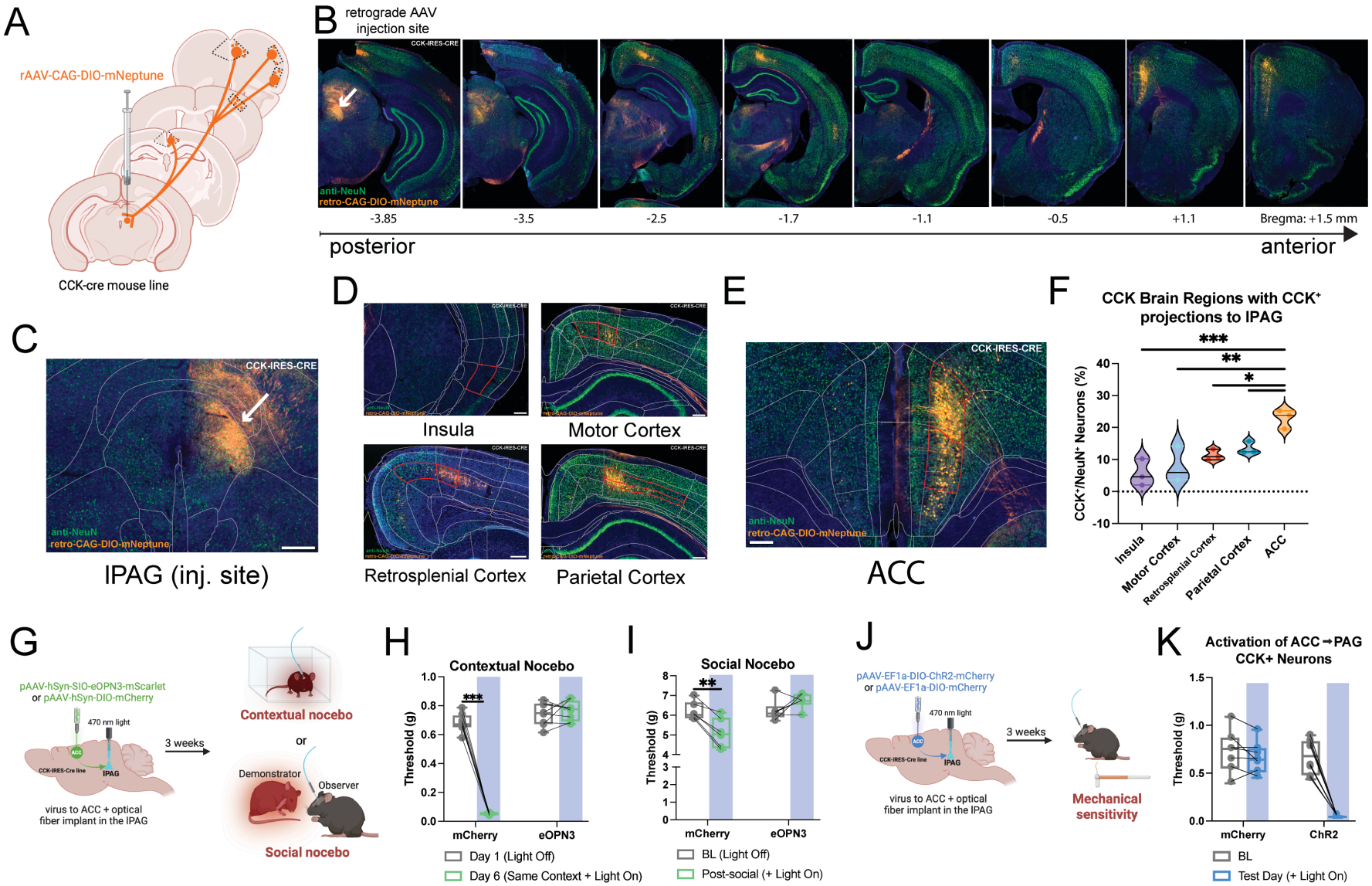
A
rAAV-CAG-DIO-mNeptune
CCK-cre mouse line
B
retrograde AAV injection site
CCK-IRES-CRE
anti-NeuN
retro-CAG-DIO-mNeptune
-3.85
-3.5
-2.5
-1.7
-1.1
-0.5
+1.1
Bregma: +1.5 mm
posterior
anterior
C
CCK-IRES-CRE
anti-NeuN
retro-CAG-DIO-mNeptune
IPAG (inj. site)
D
Insula
Motor Cortex
Retrosplenial Cortex
Parietal Cortex
E
CCK-IRES-CRE
anti-NeuN
retro-CAG-DIO-mNeptune
ACC
F
CCK Brain Regions with CCK+ projections to IPAG
CCK+/NeuN+ Neurons (%)
Insula
Motor Cortex
Retrosplenial Cortex
Parietal Cortex
ACC
G
pAAV-hSyn-SIO-eOPN3-mScarlet
or pAAV-hSyn-DIO-mCherry
470 nm light
3 weeks
virus to ACC + optical fiber implant in the IPAG
Contextual nocebo
or
Demonstrator
Observer
Social nocebo
H
Contextual Nocebo
Threshold (g)
mCherry
eOPN3
Day 1 (Light Off)
Day 6 (Same Context + Light On)
I
Social Nocebo
Threshold (g)
mCherry
eOPN3
BL (Light Off)
Post-social (+ Light On)
J
pAAV-EF1a-DIO-ChR2-mCherry
or pAAV-EF1a-DIO-mCherry
470 nm light
3 weeks
virus to ACC + optical fiber implant in the IPAG
Mechanical sensitivity
K
Activation of ACC→PAG CCK+ Neurons
Threshold (g)
mCherry
ChR2
BL
Test Day (+ Light On)

Figure 4.